Journal of Inorganic and General Chemistry
ZAAC
Zeitschrift für anorganische und allgemeine Chemie
DOI: 10.1002/zaac.201700294
ARTICLE

Uranium Oxide Nanocrystals by Microwave-Assisted Thermal Decomposition: Electronic and Structural Properties

Jennifer Leduc,[a] Joseph I. Pacold,[b] David K. Shuh,[b] Chung-Li Dong,[c] and Sanjay Mathur*[a]

Dedicated to Professor Wolfgang Schnick on the Occasion of his 60th Birthday

Abstract. Uranium oxides have attracted much attention not only in the context of nuclear energy generation but also for their application as pristine catalysts or as supports for other (transition metal) oxides and (precious) metals. Their propensity to adopt high coordination numbers and manifest multiple oxidation states (from +II to +VI) makes them attractive candidates for catalyzed transformation reactions. Herein, we report a new synthesis route to phase-pure, crystalline UO_2 nanoparticles via microwave-assisted decomposition of a molecular uranium(IV) precursor. The electronic structure and optical absorption properties of these nanocrystals were investigated using spectroscopic methods to evaluate their suitability for photo(electro)catalytic applications.

Introduction

Uranium oxides possess intrinsic electronic properties that make them attractive for electro- and photocatalytic applications. The fact that the U 5f orbitals can hybridize[1] and thus enable multiple electron transfer reactions in combination with bandgap energies in the range of 2 eV[2] make uranium oxides potential candidates for efficient photoelectrocatalysis that are effective under visible light illumination. Despite their favorable physical and chemical properties, there are only few reports on functional properties of uranium oxide nanomaterials.[3] This results mainly from the facile valence dynamics, which makes the stoichiometric control and preparation of phase pure nanomaterials rather difficult.

The pronounced valence switching of uranium oxides in combination with a high surface-to-volume ratio in nanomaterials, makes it challenging to generate uranium(IV) oxide nanocrystals with the ideal stoichiometry (U:O = 1:2), since interstitial oxygen can easily intercalate into the UO_2 fluorite lattice resulting in the formation of hyperstoichiometric UO_{2+x} ($0 < x < 0.25$).[4] There are a several examples in the literature for the synthesis of uranium oxide nanoparticles via solution-based methods.[5] A brief review of selected uranium oxide nanoparticle syntheses relevant to this report follows. In 2003, *O'Loughlin* et al. reported the formation of UO_2 nanoparticles via reduction of uranyl acetate with hydroxysulfate green rust. The obtained nanoparticles were reported to be polydisperse spheres with a diameter of 2–9 nm.[6] *Wu* et al. reported on the synthesis of monodisperse UO_2 nanoparticles via thermal decomposition of uranyl acetylacetonate in a mixture of oleic acid, oleylamine, and octadecene solutions. This reductive method generated spherical nanoparticles (ca. 5 nm) that were surface passivated by oleylamine through chelating bidentate interactions as suggested by IR spectroscopy.[7,8] *Wang* et al. prepared spherical UO_2 nanoparticles with an average diameter of 100 nm via hydrothermal reduction of uranyl acetate using ethylenediamine. The reaction was performed in an autoclave heated at 160 °C for 48 h.[9] A room temperature and surfactant-free synthesis of UO_2 nanoparticles was presented by *Nenoff* et al. in 2011.[10] The reduction of uranyl nitrate was achieved using gamma irradiation of a ^{60}Co-γ source. However, the samples needed to be exposed to the irradiation for at least 7 d.[10] All synthetic approaches described above used uranium(VI) species so that an additional in-situ reduction step for the synthesis of UO_2 nanomaterials was inevitable. The synthesis of AnO_2 nanoparticles based on An^{IV} starting materials via hydrothermal and thermal decompositions has been reported recently.[11]

In this work, we report on the straight-forward and fast (10 min) synthesis of UO_2 nanoparticles via microwave-assisted decomposition of the previously reported uranium(IV) heteroaryl alkenolate.[12] This procedure does not require an additional reduction step ($U^{VI} \rightarrow U^{IV}$) and the synthesis takes place without addition of catalysts or co-precursors. Spectroscopic investigations, such as X-ray photoelectron spectroscopy (XPS), X-ray absorption spectroscopy (XAS), spectromicroscopy, and in-situ XAS at the oxygen *K*-edge under illumination confirmed the phase composition as well as the presence of photocatalytically active orbitals in the UO_2 nanomaterial.

* Prof. Dr. S. Mathur
E-Mail: sanjay.mathur@uni-koeln.de
[a] Institute of Inorganic Chemistry
University of Cologne
50939, Cologne, Germany
[b] Chemical Sciences Division
The Glenn T. Seaborg Center
Lawrence Berkeley National Laboratory
Berkeley, California 94720, USA
[c] Department of Physics
Tamkang University
Tamsui, Taiwan
Supporting information for this article is available on the WWW under **http://dx.doi.org/10.1002/zaac.201700294** or from the author.

Results and Discussion

To synthesize UO_2 nanoparticles without an additional reduction step of uranium(VI) starting materials, a microwave-assisted decomposition using the uranium(IV) compound tetrakis[η^2-*N*,*O*-1-(4,5-dimethyl-oxazol-2-yl)-3,3,3-trifluoro-prop-en-2-olato] uranium(IV) [U(DMOTFP)$_4$] was performed. This compound exhibits preformed U–O bonds and predetermined breaking points, which enables a single-step decomposition of the precursor and nucleation of UO_2 nanocrystals. TG/DTA analysis (performed under nitrogen atmospheres) of the precursor compound revealed a decomposition temperature of ca. 267 °C and complete combustion at ca. 322 °C (Figure 1).[12] The DTA graph showed two endothermic signals in this region corresponding to the melting and evaporation processes accompanied by the loss of two DMOTFP-H ligands and two [(Me_2C_3NO)(C_2CF_3)] species. The theoretical (74.6 %) and experimentally observed (74.8 %) weight losses are in very good agreement with the formation of UO_2.

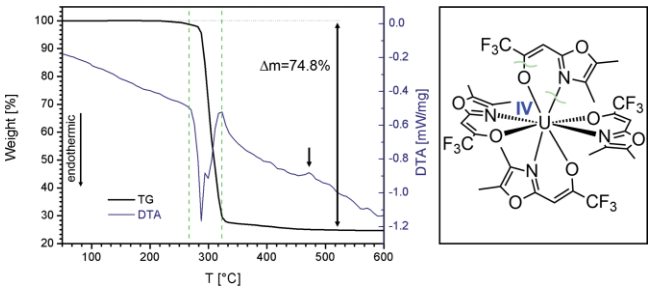

Figure 1. TG-DTA analysis of [U(DMOTFP)$_4$] performed in a nitrogen atmosphere with a heating rate of 10 K·min^{-1}. The predetermined breaking points are indicated in green.

The crystallization process occurs at 475 °C as elucidated by the small exothermic signal in the DTA. The energy required to decompose the precursor to give UO_2 nanoparticles was provided by microwave heating (electromagnetic radiation in the frequency range of 0.3 to 300 GHz). The microwave approach used in this work is suitable for high throughput synthesis with short reaction times and high yields can be achieved, while still having a precise control of reaction parameters.[13] One of these reaction parameters was the choice of the solvent. Due to the microwave heating mechanism, the selection is limited to polar solvents with a high permanent electric dipole. Water exhibits a dipole of 1.9 and thus would be appropriate to use, however, the uranium precursor is not water-soluble. In addition, water displays a boiling temperature of 100 °C, which is too low for the decomposition reaction to occur. Therefore, different solvents were screened with respect to their polarity, boiling temperatures and affinity towards solutes. The ones most suitable for the fabrication of UO_2 nanoparticles were found to be diethylene glycol (DEG), triethylene glycol (TEG), *N*-methyl-2-pyrrolidone (NMP), oleylamine, and benzyl alcohol. Preliminary tests were performed using the pure solvents and their mixtures with water. Since either no nanoparticle formation was observed (for DEG, TEG and NMP) or lower yields were obtained with pure solvents (oleylamine), further experiments were conducted using water-solvent mixtures with different ratios of the respective organic additive. A DEG:water mixture with a ratio of 4:2 was found to produce small particles (<10 nm) with a narrow size distribution and good yields. Besides precursor concentration, power, reaction temperature, and pressure, the microwave reaction time was varied from 5 to 30 min to investigate the influence on the particle size and crystallinity. As expected, the hydrodynamic diameters increased (even though only slightly, $\Delta d_{hydr} \approx$ 13 nm) with increasing reaction time. The corresponding powder X-ray diffraction (XRD) patterns (Figure 2) revealed that crystallization of UO_2 already occurred after a 10 min reaction time. With increasing reaction time enhanced crystallinity of the nanoparticles was observed, which has also been reported for the microwave-assisted synthesis of CeO_2 quantum dots.[14] In all patterns (except for the amorphous 5 min sample), the Bragg reflections were unambiguously assigned to the cubic fluorite-type UO_2 (JCPDS [36–0089]). A quantitative Rietveld refinement was performed for the sample synthesized in 30 min. The experimental powder XRD pattern (data, Figure S1, Supporting Information) was modeled using the bulk structure of UO_2[15] and the fitting (fit, Figure S1) was found to be in good agreement with the experimental data. Slight deviations result from the signal noise of the experimental pattern. The crystallite sizes, determined using the Scherrer formula from the three most intense Bragg reflections (111), (220) and (113), exhibited average crystallite sizes of 6.9 ± 0.9 nm for a reaction time of 10 min and 7.4 ± 0.2 nm for reaction times of 20 and 30 min.

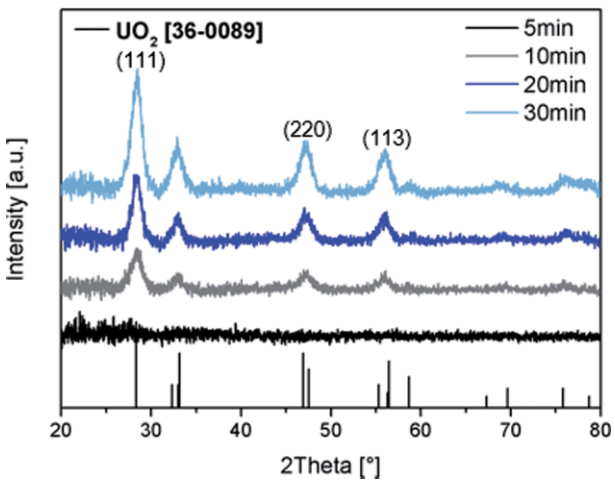

Figure 2. Powder XRD patterns of UO_2 nanoparticles synthesized with different microwave durations. The average crystallite sizes were determined using the Scherrer equation and were found to be 6.9 nm (10 min) and 7.4 nm (20, 30 min).

These results are in good agreement with the statistically determined diameters from TEM images (Figure 3). The particles synthesized with a microwave duration of 10 min are spherical and exhibit a mean size of 6.4 ± 1.2 nm. In addition, the particles reveal a relatively narrow size distribution and are crystalline as confirmed by the electron diffraction pattern (Figure S2, Supporting Information). The difference in size determined via DLS (d_{hydr} = 121 nm) and TEM or powder XRD measurements can be attributed to the agglomeration of nano-

particles. In addition, SEM images of as-prepared and washed nanoparticles (three times with a cyclohexane/ethanol mixture) revealed that these were still embedded in a residual DEG matrix. Only after further several washing steps, the excess of polymer was distinctly removed as confirmed by TEM analysis. This is consistent with literature reports on DEG-mediated microwave reactions, which show that DEG coordinates and thus, acts as a stabilizing agent during the nanoparticle synthesis. However, even after washing and drying processes, particles contained DEG residues in quantities at the level of a monolayer.[16]

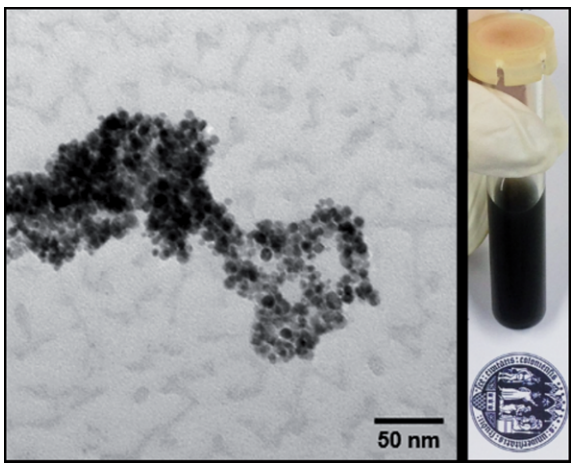

Figure 3. Transmission electron microscopy image of UO_2 nanoparticles generated via microwave decomposition of $[U(DMOTFP)_4]$ with predefined parameters: T = 220 °C, t = 10 min, p = 12 bar, c = 8.3 mg·mL^{-1}, DEG:H_2O = 4:2.

The surface characteristics of thoroughly washed UO_2 nanoparticles (synthesis time, 10 min) were investigated by FT-IR and XPS analysis. The IR spectrum (Figure 4) showed vibrational bands at 3500–3000 cm^{-1} for ν(O–H), 3000–2800 cm^{-1} for ν(CH_2), 1450–1250 cm^{-1} for δ(CH_2), and 1200–1000 cm^{-1} for ν(C–O), which is consistent with reported

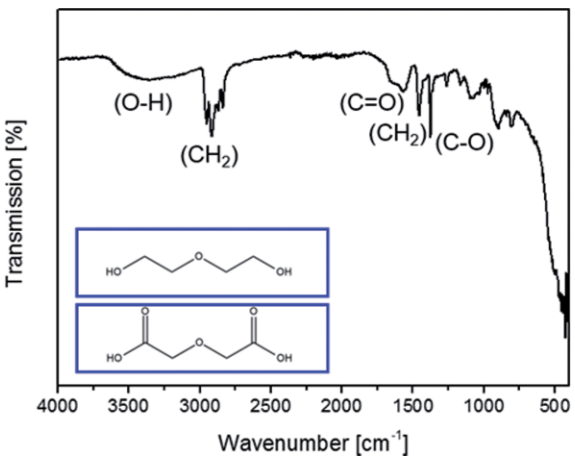

Figure 4. IR spectrum of UO_2 nanoparticles with a mean size of 6.4 ± 1.2 nm prepared via microwave decomposition of $[U(DMOTFP)_4]$. The insets show the structural formulas of DEG and diglycolic acid.

values for DEG.[17] The band at 1750–1650 cm^{-1} [ν(C=O)] corresponded to carbonyl groups, which can either be ascribed to carbonic acid formed by adsorbed atmospheric CO_2 or to diglycolic acid formed through partially oxidized DEG. There are several publications on CO_2 activation using molecular uranium compounds, in which the metal-mediated redox transformation led to formation of CO and uranium carbonate species with higher oxidized central uranium atoms.[18] The oxidation of DEG to diglycolic acid is a common step in the reduction of metal salts to give metal nanoparticles (polyol route).[19]

However, since the molecular uranium precursor already existed in the U^{IV} oxidation state, DEG did not act as reducing agent during the nanoparticle synthesis in this work. The reduction to lower valent U^{III} and U^0 species is unlikely to occur due to the high negative reduction potentials of –0.63 V and –1.70 V (Scheme 1) and the propensity of uranium(III) to disproportionate.[20]

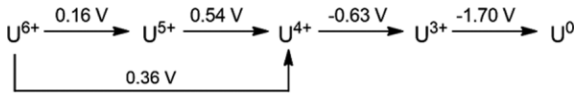

Scheme 1. Formal reduction potentials of uranium in V vs. SHE measured in 1 M $HClO_4$ at 298 K.[21]

It has been reported, that primary alcohols are decomposed at surfaces of single crystalline UO_2(111) to give the corresponding aldehyde via dehydrogenation.[22] The (111) surface exhibits the lowest surface energy and is thus the most stable surface. The powder XRD pattern of UO_2 nanoparticles synthesized herein revealed the highest intensity in the (111) Bragg reflection and thus oxidation of DEG at the UO_2 nanoparticle surfaces is likely to occur to a certain degree. When any residual solvents were removed by several washing steps, the deprotonated diglycolic acid acts as stabilizer for the UO_2 nanoparticles. UO_2 is characterized by two very broad bands at 340 and 470 cm^{-1} in the IR spectrum. However, since DEG exhibits a band in this region, an assignment of UO_2 is difficult. In contrast, the higher oxides of uranium (U_4O_9, α-U_3O_8, UO_3) all show a characteristic band at 740 cm^{-1}, which corresponds to stretching vibrations of the U–O bond in the –O–U–O–U– chain, and was used by *Allen* et al. to distinguish binary uranium oxides with different U:O ratios.[23] Since this band was absent in the IR spectrum of the synthesized UO_2 nanoparticles, the presence of higher oxidized uranium species can be excluded. Thus, the presence of organic surfactants might stabilize the central U^{IV} atom since no oxidation of U^{IV} is observed despite atmospheric conditions during the microwave reaction.

The XPS survey scan (Figure 5a) of the UO_2 nanoparticles showed solely signals for carbon (61.0 at.%), oxygen (32.8 at.%), and uranium (6.2 at.%). The high carbon content indicates the adsorption of DEG at the UO_2 nanoparticle surface, which is consistent with the IR results. Neither nitrogen nor fluorine was detected, pointing toward a clean decomposition of the molecular uranium compound. To obtain detailed information on the oxidation state of uranium, the two U $4f_{5/2}$ and U $4f_{7/2}$ signals in the high-resolution U 4f spectrum (Fig-

ure 5b) and the O 1s signal (Figure 5c) in the binding energy range of 536–522 eV were investigated. The peak energies of the U $4f_{5/2}$ and U $4f_{7/2}$ are in good agreement with literature reported values[24] for single crystal UO_2 thin films (Table S1, Supporting Information). The shake-up satellites, which are characteristic for UO_2 and should exhibit a distance of 6.9 eV from the basic U 4f signal, are observed at 384.58 eV and 396.00 eV. The large FWHM of both the U 4f and O 1s signals could arise from the coordination of DEG to the nanoparticle surface; the existence of higher oxidized uranium species was ruled out by IR analysis. This would be consistent with the shift of the O 1s signal toward lower peak energies.

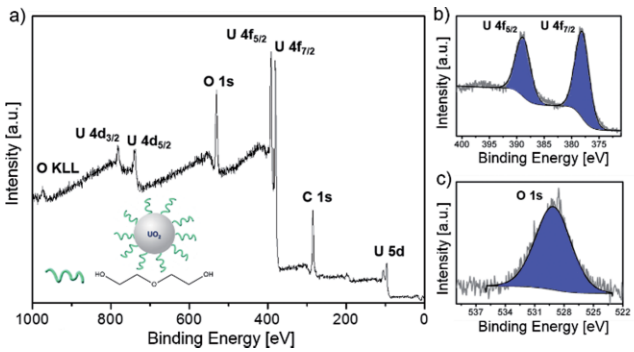

Figure 5. (a) Survey XPS scan and high resolution XPS spectra of (b) U 4f and (c) O 1s states of thoroughly washed UO_2 nanoparticles with a mean size of 6.4 ± 1.2 nm. The signals in the high-resolution spectra were fit by a Gaussian-Lorentzian function.

To unambiguously determine the oxidation state of the synthesized nanomaterials, XAS spectromicroscopy was performed. For this purpose, UO_2 nanoparticles were dispersed in ethanol and drop coated onto a Si_3N_4 membrane. Since the particles were stored in ethanol for a period of three months without sonication, the agglomeration had progressed further. The STXM images (at different magnifications) and the corresponding O XAS spectrum collected from the particles shown in (c) are displayed in Figure 6. A series of images was collected in an energy range from 510.0–570.0 eV for the oxygen *K*-edge. The signal collected from the particles (dark areas) was normalized to the photon flux extracted from the Si_3N_4 window (bright area, low level of absorption). The background was subtracted from the resulting spectrum and the decomposition of the peaks was performed using a Gaussian fitting methodology.

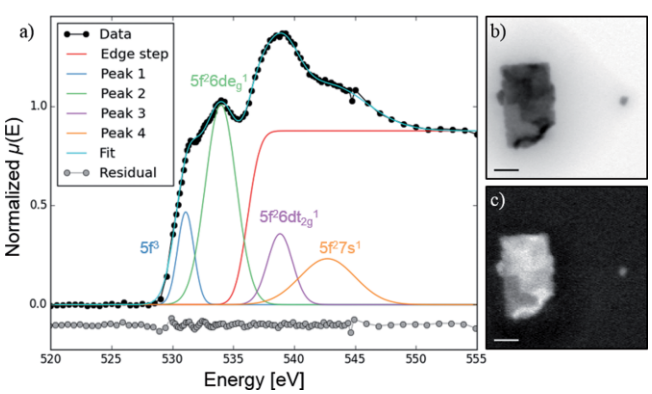

Figure 6. (a) Decomposition of the O *K*-edge spectrum acquired from UO_2 nanoparticles deposited from an ethanol dispersion, shown with a fit consisting of a sum of an arctan function and four Gaussian peaks. (b) Scanning transmission X-ray micrograph of agglomerated UO_2 nanoparticles acquired with a photon energy of 728 eV. Scale bar, 1 micron. (c) Uranium map of the region shown in (b), generated by measuring the difference in absorbance at 728 eV and 740 eV.

The peak positions are in agreement with the energies reported for polycrystalline UO_2 powders by *Jollet* et al.[25] UO_2 crystallizes in the cubic space group $Fm\bar{3}m$ and exhibits a formal ionic ground state configuration of U $6p^6 5f^2 6d^0 7s^0$ O $2p^6$, which can be abbreviated as $5f^2$. For the oxygen *K*-edge XAS, an oxygen 1s electron is promoted to the empty oxygen 2p levels, which results in an oxygen 1s hole and a mixture of uranium $5f^3$ and $5f^2 6d^1$configurations. Since in a cubic crystal field, the d orbitals are split into e_g (lower energy) and t_{2g} (higher energy) orbitals, two configurations are possible for the $5f^2 6d^1$ configuration, i.e. $5f^2 6de_g^1$ and $5f^2 6dt_{2g}^1$. These configurations were attributed to peaks 2 and 3. Peak 1 and the small shoulder towards lower energies, which results from spin-orbit splitting, were assigned to the hybridized $5f^3$ states. In accordance with simulated data, the hybridized U 5f states are lower in energy than the U 6d ones.[25] In addition, the U 5f-O 2p hybridization is smaller than the U 6d-O 2p hybridization as indicated by the lower intensity of peak 1 compared to peaks 2 and 3. The very broad signal at energies higher than 540 eV (peak 4) was attributed to hybridized 7s(7p)-O 2p states.

In-situ XAS in the dark and under light illumination at the oxygen *K*-edge of powder-dried UO_2 nanoparticles with a mean size of 6.4 ± 1.2 nm was performed to evaluate the photocatalytically active orbitals. As previously reported, the spectral features strongly depend on the preparation method.[26] In case of the UO_2 powder, the signals corresponding to the hybridized uranium $5f^3$ states were more pronounced than in the dispersed sample. In Figure 6 and the reference spectrum by *Jollet* et al., the $5f^3$ states appear as "shoulders" towards lower energies of the $5f^2 6de_g^1$ signal, whereas in the UO_2 powder both signals are distinguishable and exhibit comparable intensities (Figure 7). Upon illumination with incident light (350–

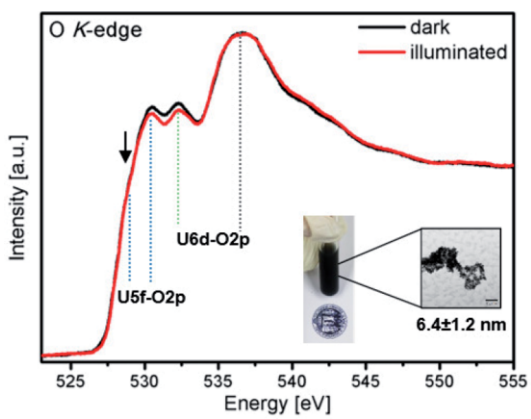

Figure 7. In-situ XAS spectrum in the dark (black) and under illumination (red) of UO_2 nanoparticles with a mean size of 6.4 ± 1.2 nm prepared in this work via microwave-assisted decomposition.

750 nm), both the $5f^3$ and $5f^2 6de_g^1$ states show decreased intensity, whereas the $5f^2 6dt_{2g}^1$ is not affected. Since the intensity of the signals is directly proportional to the amount of unoccupied states, light illumination promotes charge carrier dynamics at these sites.

The decreased intensity may imply that electrons are excited from the valence band to the conduction band under illuminated conditions. Thus, UO_2 exhibits properties allowing the study of its possible application as a photocatalyst, which has been the subject of other studies, not in the focus of this work, in our group. In addition, the optical absorbance of the UO_2 nanoparticles with a mean size of 6.4 ± 1.2 nm was investigated by UV/Vis-spectroscopy. The broad non-symmetric band between 250 and 500 nm (Figure S3, Supporting Information) consists of at least two signals which is consistent with reported spectra for UO_2.[27] The band maximum at 218 nm corresponds to the $5f^2 \rightarrow 6dt_{2g}5f^1$ transition, while the lower energy band can be assigned to the $5f^2 \rightarrow 6de_g5f^1$ transition with a shoulder from spin orbit splitting.[28] However, DEG also exhibits an absorption band with a maximum at ca. 325 nm. Charge-transfer transitions ($2p \rightarrow 6de_g$) occur at higher photon energies (ca. 8 eV).[28] Whereas the oxygen *K*-edge XAS measurements suggest a f–f type band transition, the optical spectra propose that UO_2 is a f–d type since upon excitation neither the O 2p nor the U 5f electrons can access the unoccupied 5f state but only the unoccupied 6d state according to dipole selection rules.[29] The bandgap of the material was determined using the Tauc formula for direct bandgap materials. The linear part of $(ah\upsilon)^2$ vs. $h\upsilon$ extrapolated to the baseline yielded the value of the bandgap (inset Figure S3, Supporting Information). Bulk UO_2 was reported to exhibit a bandgap of 2–2.3 eV.[2] The higher value of 2.5 eV found for UO_2 nanoparticles is likely explained by the quantum confinement effect.

To investigate the role of the microwave method compared to pure thermolysis, the following experiments were performed: (a) thermal decomposition of $[U(DMOTFP)_4]$ at 330 °C in air, (b) heating up the precursor in DEG to 330 °C and (c) hot-injection of a solution of $[U(DMOTFP)_4]$ in oleylamine into preheated (350 °C) trioctyl phosphine (TOP).[30] Whereas simple heating of the precursor only yielded a black, amorphous powder, both thermolysis in air and hot-injection resulted in the formation of crystalline UO_2 as shown by XRD analysis (Figure S4, Supporting Information). The higher intensity of the diffraction peaks in the sample prepared via pure thermolysis is likely explained by the formation of bulk UO_2 due to the sintering effect. The average crystallite size of the sample prepared via hot-injection was determined to be 9.1 ± 0.3 nm using the Scherrer formula. Although both hot-injection and microwave decomposition produced small particles (<10 nm), the microwave approach was deemed more suitable as it drastically shortened the reaction time and temperature, while still retaining a precise control of size, shape, composition, and crystal phase.

Conclusions

In this contribution, we have presented the fast and simple synthesis of phase pure UO_2 nanoparticles via microwave assisted decomposition of the uranium(IV) complex $[U(DMOTFP)_4]$ without the need of additional reducing agent or co-catalyst. The particles show a narrow size distribution of 6.4 ± 1.2 nm. XAS studies, the bandgap value of 2.5 eV and the overall absorption in the visible light region as well as the existence of optoelectronically active hybridized U 5f-O 2p and U 6d-O 2p states, point towards the possible implementation of UO_2 nanomaterials for photo(electro)catalytic applications.

Experimental Section

Chemicals: Diethylene glycol (DEG, 99.5 %, Acros), ethanol (absolute, Merck), oleylamine (97 %, Acros), trioctyl phosphine (97 %, Sigma Aldrich) and cyclohexane (p.a., Sigma Aldrich) were used as received without further purification. The synthesis and chemical characterization of tetrakis[η^2-*N*,*O*-1-(4,5-dimethyl-oxazol-2-yl)-3,3,3-trifluoropropen-2-olato] uranium(IV) $[U(DMOTFP)_4]$ was performed according to literature procedure.[12]

Synthesis of UO_2 Nanocrystals: For the preparation of UO_2 nanoparticles all solvents were degassed prior to use to prevent oxidation of the precursor. Standard procedure: In a 25 mL flask 50 mg of $[U(DMOTFP)_4]$ were dispersed in 4 mL DEG. The green dispersion was transferred to a microwave tube equipped with a stirring bar. Just before the start of the microwave reaction, 2 mL of water were added. The microwave parameters were adjusted (dynamic mode, 50 W, 12 bar, 220 °C) and the reaction time was set to 10 min. Subsequently, the black dispersion was transferred to a centrifuge tube and centrifuged for 15 min at 11000 rpm. The supernatant was decanted and the black precipitation was washed with an ethanol/cyclohexane (25 ml/15 mL) mixture and sonicated for 10 min prior to centrifuging again. This washing cycle was repeated for 3 times, then repeated with 40 mL of ethanol, and finally with 40 mL of water. After the last step, the samples were redispersed in ethanol for further analysis. Microwave decompositions were performed in a Discovery S system (CEM) in 10 mL glass pressure vessels and in the dynamic mode.

Thermal Decomposition of $[U(DMOTFP)_4]$ in DEG: $[U(DMOTFP)_4]$ (50 mg) was dispersed in DEG (4 mL) and heated to 140 °C under vacuum for 20 min. Subsequently, the mixture was heated to 330 °C in a nitrogen atmosphere and refluxed for 20 min. After the mixture was cooled to room temperature, the brown dispersion was transferred to a centrifuge tube and centrifuged for 15 min at 11000 rpm. The supernatant was decanted and the brown precipitate was washed with an ethanol/cyclohexane (25 ml/15 mL) mixture and sonicated for 10 min prior to centrifuging again. This washing cycle was repeated for 3 times, then repeated with 40 mL of ethanol, and finally with 40 mL of water. After the last step, the samples were dried for XRD analysis.

Thermolysis of $[U(DMOTFP)_4]$: $[U(DMOTFP)_4]$ (50 mg) was heated to 330 °C under air for 10 h at a heating rate of 10 K·min^{-1}.

Hot Injection Method: $[U(DMOTFP)_4]$ (200 mg) was suspended in oleylamine (10 mL). The mixture was heated to 140 °C and stirred for 1 h, resulting in a brown solution. Subsequently, the solution was injected to 8 mL trioctyl phosphine, which was preheated to 350 °C. The mixture was stirred for 45 min at this temperature. Subsequently, the orange dispersion was transferred to a centrifuge tube and centrifuged for 15 min at 11000 rpm. The supernatant was decanted and the black precipitate was washed with an ethanol/cyclohexane (25 ml/15 mL)

mixture and sonicated for 10 min prior to centrifuging again. This washing cycle was repeated for 3 times, then repeated with 40 mL of ethanol, and finally with 40 mL of water. After the last step, the samples were dried for XRD analysis

Characterization: TGA/DTA measurements were performed with a STARe-system from Mettler-Toledo, equipped with a TGA/DTA1 unit and a GC100 gas controller. UV/Vis spectra were recorded with a Lambda 950 (Perkin-Elmer) device. FT-IR spectra were recorded with a Spectrum 400 (Perkin-Elmer) instrument. X-ray photoelectron spectroscopy (XPS) measurements were carried out using a spectrometer (Φ 5600ci, Perkin-Elmer) at a pressure below 10^{-8} mbar under a non-monochromatic Al-K_α excitation source (186.6 eV) with an ESCA M-Probe spectrometer (Surface Science Instruments SSI). Correction to the binding energies was done in reference to the C1s-signal (284.8 eV). Spectral corrections and composition calculations were performed using CasaXPS. TEM measurements were carried out using a ZEISS LEO 902 microscope operating at 120 kV with LaB_6 cathode in a bright field mode. The samples were deposited onto a carbon coated copper grid. The mean diameter was statistically determined from a varying number of nanoparticles from bright field micrographs. The hydrodynamic radii of the particles were measured with a Malvern Instruments Zetasizer Nano ZS (operating wavelength: 633 nm). XRD measurements were performed on a STOE-STADI P using either Cu-K_α radiation (λ = 1.5418 Å) or Mo-K_α-radiation (λ = 0.7093 Å). The in-situ XAS measurements of the O *K*-edge were carried out in TEY mode at BL20A1 at the National Synchrotron Radiation Research Center in Taiwan. The spectra were recorded in the dark and under illumination (1.5 AM solar simulator, HAL-302, Asahi Spectra, Japan). XAS measurements were performed at the scanning transmission X-ray microscope (STXM) end station of the Advanced Light Source-Molecular Environmental Sciences Beamline 11.0.2 at the Lawrence Berkeley National Laboratory in Berkeley, CA, USA.[31]

Supporting Information (see footnote on the first page of this article): The Supporting Information includes the Rietveld refinement, electron diffraction pattern, TEM image and UV-vis spectra of UO_2 nanoparticles prepared via microwave decomposition. In addition, XRD patterns of UO_2 materials synthesized via thermal decomposition are displayed.

Acknowledgements

The authors would like to acknowledge the University of Cologne for providing the infrastructural support and the Deutsche Forschungsgemeinschaft (DFG) for funding obtained within the priority program SPP 1613 “Fuels Produced Regeneratively Through Light-Driven Water Splitting” and financial assistance by the Fonds der Chemischen Industrie (VCI) (for J•L.). We thank Dr. Erik Strub and Uwe Otto from the nuclear chemistry division for support throughout the whole project. The STXM spectromicroscopy, JIP, and DKS were supported by the Director, Office of Science, Office of Basic Energy Sciences, Division of Chemical Sciences, Geosciences, and Biosciences (CSGB) Heavy Elements Chemistry program of the U.S. Department of Energy (DOE) under Contract Number DE-AC02–05CH11231 at LBNL. This research used resources of the Advanced Light Source, which is a DOE Office of Science User Facility under Contract no. DE-AC02–05CH11231 at LBNL.

Keywords: In-situ X-ray absorption spectroscopy; Scanning transmission X-ray microscopy (STXM); Photocatalysis; Uranium; UO_2 nanoparticles; Microwave chemistry

References

[1] J. M. Boncella, *Nature* **2008**, *451*, 250–252.
[2] H. Idriss, *Surf. Sci. Rep.* **2010**, *65*, 67–109.
[3] W. Q. Shi, L. Y. Yuan, Z. J. Li, J. H. Lan, Y. L. Zhao, Z. F. Chai, *Radiochim. Acta* **2012**, *100*, 727–736.
[4] H. He, D. Shoesmith, *Phys. Chem. Chem. Phys.* **2010**, *12*, 8109–8118.
[5] a) P. Chen, D. Y. Huang, C. C. Chen, T. Suzuki-Muresan, M. L. Kang, J. Wang, G. Song, B. A. Wang, *J. Radioanal. Nucl. Chem.* **2017**, *313*, 229–237; b) M. Leblanc, J. Causse, Z. J. Lu, D. Rebiscoul, *Colloids Surf. A* **2017**, *522*, 18–27; c) I. Majumder, S. Chatterjee, R. C. Fischer, S. K. Neogi, F. A. Mautner, T. Chattopadhyay, *Inorg. Chim. Acta* **2017**, *462*, 112–122; d) N. Mohseni, S. J. Ahmadi, M. Roshanzamir, M. Najafi, S. M. Mirvakili, *Ceram. Int.* **2017**, *43*, 3025–3034; e) R. Jovani-Abril, M. Gibilaro, A. Janssen, R. Eloirdi, J. Somers, J. Spino, R. Malmbeck, *J. Nucl. Mater.* **2016**, *477*, 298–304; f) D. K. Hwang, T. Tsukahara, K. Tanaka, M. Osaka, Y. Ikeda, *J. Nucl. Mater.* **2015**, *466*, 134–141; g) R. Zhao, L. Wang, Z.-J. Gu, L.-Y. Yuan, C.-L. Xiao, Y.-L. Zhao, Z.-F. Chai, W.-Q. Shi, *CrystEngComm* **2014**, *16*, 2645–2651; h) L. Wang, R. Zhao, C. Z. Wang, L. Y. Yuan, Z. J. Gu, C. L. Xiao, S. A. Wang, X. W. Wang, Y. L. Zhao, Z. F. Chai, W. Q. Shi, *Chem. Eur. J.* **2014**, *20*, 12655–12662.
[6] E. J. O’Loughlin, S. D. Kelly, R. E. Cook, R. Csencsits, K. M. Kemner, *Environ. Sci. Technol.* **2003**, *37*, 721–727.
[7] H. Wu, Y. Yang, Y. C. Cao, *J. Am. Chem. Soc.* **2006**, *128*, 16522–16523.
[8] D. Hudry, C. Apostolidis, O. Walter, T. Gouder, E. Courtois, C. Kübel, D. Meyer, *Chem. Eur. J.* **2013**, *19*, 5297–5305.
[9] Q. Wang, G.-D. Li, S. Xu, J.-X. Li, J.-S. Chen, *J. Mater. Chem.* **2008**, *18*, 1146–1152.
[10] T. M. Nenoff, B. W. Jacobs, D. B. Robinson, P. P. Provencio, J. Huang, S. Ferreira, D. J. Hanson, *Chem. Mater.* **2011**, *23*, 5185–5190.
[11] a) O. Walter, K. Popa, O. D. Blanco, *Open Chem.* **2016**, *14*, 170–174; b) N. Clavier, J. Maynadie, A. Mesbah, J. Hidalgo, R. Lauwerier, G. I. N. Bouala, S. Parres-Maynadie, D. Meyer, N. Dacheux, R. Podor, *J. Nucl. Mater.* **2017**, *487*, 331–342; c) V. Tyrpekl, M. Cologna, D. Robba, J. Somers, *J. Eur. Ceram. Soc.* **2016**, *36*, 767–772; d) V. Tyrpekl, J. F. Vigier, D. Manara, T. Wiss, O. D. Blanco, J. Somers, *J. Nucl. Mater.* **2015**, *460*, 200–208.
[12] L. Appel, J. Leduc, C. L. Webster, J. W. Ziller, W. J. Evans, S. Mathur, *Angew. Chem. Int. Ed.* **2015**, *54*, 2209–2213.
[13] L. S. Xiao, H. Shen, R. von Hagen, J. Pan, L. Belkoura, S. Mathur, *Chem. Commun.* **2010**, *46*, 6509–6511.
[14] T. Lehnen, J. Schlafer, S. Mathur, *Z. Anorg. Allg. Chem.* **2014**, *640*, 819–825.
[15] M. Freyss, *Phys. Rev. B* **2010**, *81*, 014101.
[16] C. Feldmann, S. Matschulo, S. Ahlert, *J. Mater. Sci.* **2007**, *42*, 7076–7080.
[17] E. Hammarberg, A. Prodi-Schwab, C. Feldmann, *Thin Solid Films* **2008**, *516*, 7437–7442.
[18] O. Cooper, C. Camp, J. Pecaut, C. E. Kefalidis, L. Maron, S. Gambarelli, M. Mazzanti, *J. Am. Chem. Soc.* **2014**, *136*, 6716–6723.
[19] D. S. Li, S. Komarneni, *J. Am. Ceram. Soc.* **2006**, *89*, 1510–1517.
[20] S. T. Liddle, *Angew. Chem. Int. Ed.* **2015**, *54*, 8604–8641.
[21] H. S. La Pierre, M. Rosenzweig, B. Kosog, C. Hauser, F. W. Heinemann, S. T. Liddle, K. Meyer, *Chem. Commun.* **2015**, *51*, 16671–16674.
[22] S. V. Chong, M. A. Barteau, H. Idriss, *Catal. Today* **2000**, *63*, 283–289.
[23] G. C. Allen, N. R. Holmes, *Appl. Spectrosc.* **1994**, *48*, 525–530.
[24] M. M. Strehle, B. J. Heuser, M. S. Elbakhshwan, X. Han, D. J. Gennardo, H. K. Pappas, H. Ju, *Thin Solid Films* **2012**, *520*, 5616–5626.
[25] F. Jollet, T. Petit, S. Gota, N. Thromat, M. Gautier-Soyer, A. Pasturel, *J. Phys. Condens. Matter* **1997**, *9*, 9393–9401.

[26] S. D. Conradson, D. A. Andersson, P. S. Bagus, K. S. Boland, J. A. Bradley, D. D. Byler, D. L. Clark, D. R. Conradson, F. J. Espinosa-Faller, J. S. Lezama Pacheco, M. B. Martucci, D. Nordlund, G. T. Seidler, J. A. Valdez, *Nucl. Instrum. Methods Phys. Res. Sect. B* **2016**, *374*, 45–50.
[27] R. J. Ackermann, R. J. Thorn, G. H. Winslow, *J. Opt. Soc. Am.* **1959**, *49*, 1107–1111.
[28] J. Schoenes, *J. Appl. Phys.* **1978**, *49*, 1463–1465.
[29] S. W. Yu, J. G. Tobin, J. C. Crowhurst, S. Sharma, J. K. Dewhurst, P. Olalde-Velasco, W. L. Yang, W. J. Siekhaus, *Phys. Rev. B* **2011**, *83*, 165102.
[30] C. D. Donega, P. Liljeroth, D. Vanmaekelbergh, *Small* **2005**, *1*, 1152–1162.
[31] H. Bluhm, K. Andersson, T. Araki, K. Benzerara, G. E. Brown Jr., J. J. Dynes, S. Ghosal, H.-Ch. Hansen, J. C. Hemminger, A. P. Hitchcock, G. Ketteler, E. Kneedler, J. R. Lawrence, G. G. Leppard, J. Majzlam, B. S. Mun, S. C. B. Myneni, A. Nilsson, H. Ogasawara, D. F. Ogletree, K. Pecher, D. K. Shuh, M. Salmeron, B. Tonner, T. Tyliszczak, T. H. Yoon, *J. Electron. Spectros. Relat. Phenom.* **2006**, *150*, 86–104.

Received: August 14, 2017
Published online: December 1, 2017

